The Partitioning of Evapotranspiration into Transpiration, Soil Evaporation, and Canopy Evaporation in a GCM: Impacts on Land–Atmosphere Interaction

DAVID M. LAWRENCE, PETER E. THORNTON, KEITH W. OLESON, AND GORDON B. BONAN

National Center for Atmospheric Research, Boulder, Colorado*

(Manuscript received 28 December 2005, in final form 13 November 2006)

ABSTRACT

Although the global partitioning of evapotranspiration (ET) into transpiration, soil evaporation, and canopy evaporation is not well known, most current land surface schemes and the few available observations indicate that transpiration is the dominant component on the global scale, followed by soil evaporation and canopy evaporation. The Community Land Model version 3 (CLM3), however, does not reflect this global view of ET partitioning, with soil evaporation and canopy evaporation far outweighing transpiration. One consequence of this unrealistic ET partitioning in CLM3 is that photosynthesis, which is linked to transpiration through stomatal conductance, is significantly underestimated on a global basis. A number of modifications to CLM3 vegetation and soil hydrology parameterizations are described that improve ET partitioning and reduce an apparent dry soil bias in CLM3. The modifications reduce canopy interception and evaporation, reduce soil moisture stress on transpiration, increase transpiration through a more realistic canopy integration scheme, reduce within-canopy soil evaporation, eliminate lateral drainage of soil water, increase infiltration of water into the soil, and increase the vertical redistribution of soil water. The partitioning of ET is improved, with notable increases seen in transpiration (13%–41% of global ET) and photosynthesis (65–148 Pg C yr^{-1}). Soils are wetter and exhibit a far more distinct soil moisture annual cycle and greater interseasonal soil water storage, which permits plants to sustain transpiration through the dry season.

The broader influences of improved ET partitioning on land–atmosphere interaction are diverse. Stronger transpiration and reduced canopy evaporation yield an extended ET response to rain events and a shift in the precipitation distribution toward more frequent small- to medium-size rain events. Soil moisture memory time scales decrease particularly at deeper soil levels. Subsurface soil moisture exerts a slightly greater influence on precipitation. These results indicate that partitioning of ET is an important responsibility for land surface schemes, a responsibility that will gain in relevance as GCMs evolve to incorporate ever more complex treatments of the earth's carbon and hydrologic cycles.

1. Introduction

One of the primary roles of a land surface scheme in a global climate model (GCM) is to partition surface available energy into latent and sensible heat fluxes. Determination of latent heat flux, which is directly proportional to total evapotranspiration (ET), is more involved than for sensible heat flux since it is the sum of transpiration (E_T), soil evaporation (E_S), and canopy evaporation (E_C). The relative contribution of each component of ET is calculated within the land surface scheme relative to potential evaporation according to independent resistances to evaporation for each component due to turbulent transfer, moisture limitations, and, in the case of transpiration, stomatal physiology.

Global- and regional-scale partitioning of ET is not accurately known since large-scale observations of ET, let alone its partitioning, are simply not available. Perhaps as a consequence, few researchers have diagnosed ET partitioning in land surface schemes, even though it would provide a powerful constraint on model physics. Choudhury and DiGirolamo (1998) and Choudhury et al. (1998) use a biophysical process-based model forced with observed precipitation, air temperature, net radiation, and vapor pressure deficit to derive global climatological quantities for ET and ET partitioning. They

* The National Center for Atmospheric Research is sponsored by the National Science Foundation.

Corresponding author address: David M. Lawrence, NCAR, P.O. Box 3000, Boulder, CO 80307-3000.
E-mail: dlawren@ucar.edu

DOI: 10.1175/JHM596.1

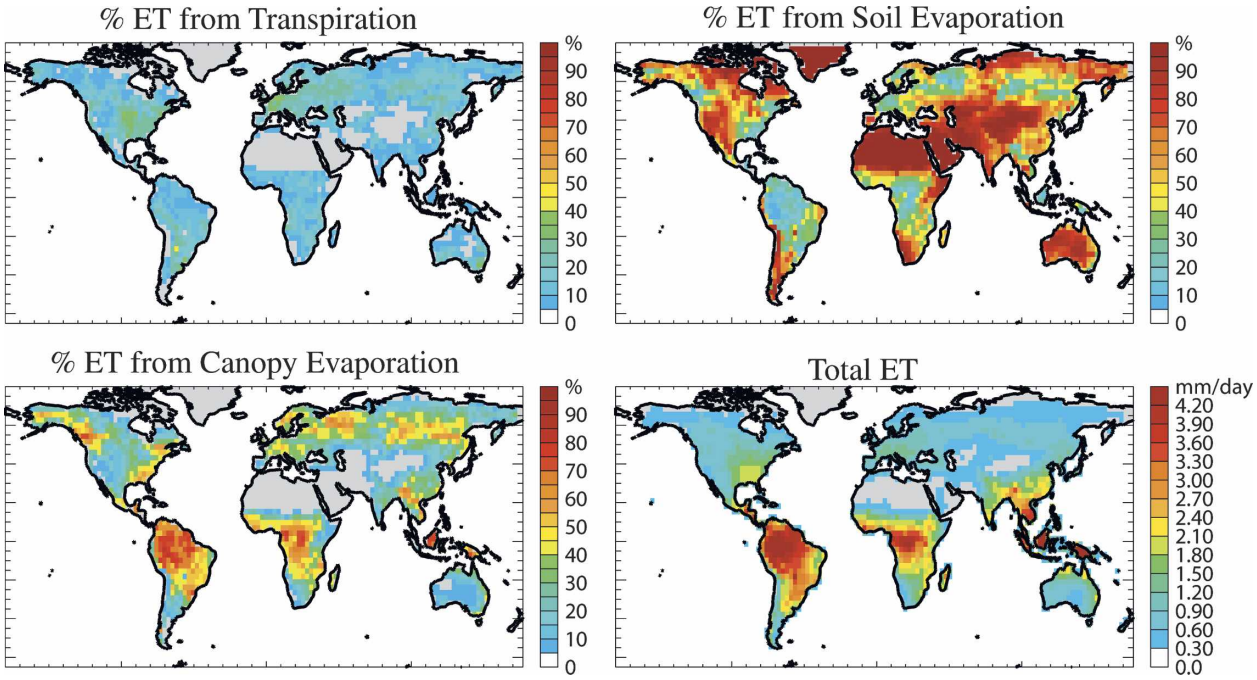

FIG. 1. Percent of annual mean ET from transpiration, soil evaporation, and canopy evaporation, respectively, and total ET for the offline CLM3 control simulation ($CONTROL_{off}$).

find that E_T accounts globally for about 52% of total ET while E_S contributes 28% and E_C the remaining 20%. A more recent estimate of global ET partitioning is obtained from multimodel output from the Global Soil Wetness Project 2 (GSWP2; Dirmeyer et al. 2005). In GSWP2, the multimodel mean estimate of global ET partitioning is 48% E_T, 36% E_S, and 16% E_C.

Strict validation of a global land surface model's ET partitioning is not possible because field measurements of ET partitioning are very sparse. Transpiration and soil evaporation can be isolated either through a combination of stable isotope, sap flow, and eddy covariation techniques (Williams et al. 2004) or with porometer, lysimeter, and Bowen ratio techniques, although errors in ET partitioning calculated by any of these methods may be large (Herbst et al. 1996). A literature survey reveals only a limited number of studies that report ET partitioning. It is difficult to extract clear and useful guidance for GCM development from these disparate studies, although it is reasonable to interpret that transpiration is the dominant component of ET across a variety of ecohydrological systems (Wallace et al. 1993; Ashktorab et al. 1994; Leuning et al. 1994; Black et al. 1996; Wilson et al. 2001; Ferretti et al. 2003; Williams et al. 2004). However, when the canopy is sparse, the partitioning is more complex (Baldocchi et al. 2004) and soil evaporation can at times dominate (Allen 1990; Yunusa et al. 1997).

By comparison to other models, and the limited observations, the Community Land Model version 3 (CLM3) partitions ET in an unrealistic manner. Averaged over the global land surface, ET partitioning in CLM3, when forced by observed meteorology, is 13% E_T, 44% E_S, and 43% E_C (Fig. 1 shows the geographic distribution of ET partitioning). The partitioning is just as unrealistic when CLM3 is coupled to the Community Atmosphere Model version 3 (CAM3) (11% E_T, 57% E_S, and 32% E_C). This unrealistic partitioning of ET is likely to affect both mean ET and its temporal evolution. Since the time scales of response differ for each ET component (fast for E_C, slower for E_S, and slowest for E_T), the time scale of ET response and the local climate response, such as to a rainfall event or a seasonal precipitation anomaly, is likely to be affected by how CLM3 executes the partitioning. Weak E_T also may affect the amplitude and regionality of CAM3–CLM3 land–atmosphere coupling. Transpiration by plants is also critically important due to its interactive role in photosynthetic gas exchange and productivity. As an example, when CLM3 is coupled to a dynamic global vegetation model, weak E_T spawns conversion of forests to grassland in areas where forests should dominate, such as in Amazonia and the southeastern United States (Bonan and Levis 2006). Low photosynthesis during the Amazonian dry season prevents establishment of a broadleaf evergreen forest; instead a decidu-

ous forest dominates. For all of these reasons, a substantial improvement to ET partitioning is important within the context of ongoing development goals of the Community Climate System Model version 3 (CCSM3) with respect to modeling the hydrologic cycle (Hack et al. 2006) and the carbon cycle (Thornton and Zimmerman 2007).

In this paper we describe a series of simple modifications to CLM3 hydrology and vegetation parameterizations that together substantially improve the partitioning of ET in both offline and coupled configurations through reduced canopy interception, increased soil moisture availability for transpiration, and increased soil moisture storage. We also evaluate how the partitioning of ET affects climate simulations with an emphasis on how ET partitioning influences land–atmosphere interactions. It should be noted that this research has been conducted within the context of a longer-term CLM community-oriented project that is focused on a thorough reconsideration, evaluation, and development of CLM hydrology. The modifications documented here represent significant practical improvements to the released version of CLM3, thereby providing an interim model version that can be used by researchers and model developers while a new hydrology scheme for CLM is developed.

2. Model description

We use CLM3 in both offline mode and coupled to CAM3 (Collins et al. 2006). CLM3 is described in detail in Oleson et al. (2004) and its performance is documented in Dickinson et al. (2006). Subgrid-scale surface-type heterogeneity is represented in CLM3 through satellite-derived fractional coverage of lakes, wetland, bare soil, glacier, and vegetation consisting of up to four plant functional types in each grid box. Fluxes of energy and moisture are modeled independently for each surface type and aggregated before being passed to the atmosphere model. The four plant functional types share a single soil column, with 10 soil layers extending to 3.43-m depth (layer depths increase exponentially from 0.0175 m at the top to 1.14 m at the bottom). Soil moisture heterogeneity is simply represented through differing runoff formulations for the saturated and unsaturated fractions of the soil column, which are dynamically defined according to water table depth. Further details of CLM3 directly relevant to the ET partitioning are described in the following section.

3. Modifications to model physics

In this section we describe a series of modifications to CLM3 model physics and parameterizations that result in a more reasonable partitioning of ET, as well as wetter soils and greater interseasonal soil water storage. The use of the somewhat ambiguous term "more reasonable" is deliberate. As noted in the introduction, strict validation of a global model's ET partitioning is not possible because the required observations do not exist. The few local-scale observations of ET partitioning can, at best, provide limited guidance on the relative importance of E_T, E_S, and E_C for various ecosystems. Hence, we consider the multimodel global offline results provided in GSWP2 (Dirmeyer et al. 2005) to be the scientific communities' current best estimate of ET partitioning, and we use these values as a soft target to partially direct the model changes. To further constrain the modifications to CLM3, we require that the runoff simulation, for which there is validation data, is not degraded. Note again that although the changes outlined here, to the extent possible, are physically realistic and defensible solutions to correct known deficiencies in model behavior, the changes are also motivated strongly by an urgent need for a more reasonable representation of ET partitioning and soil hydrology that will permit ongoing hydrologic and carbon cycle model development while a more thorough reconsideration of CLM hydrology is undertaken.

The changes are presented as serial modifications to the original model (CONTROL) and are tested and evaluated for their impact on ET partitioning and runoff in offline mode. Each model configuration is run for 15 yr (1987–2001), forced with observed precipitation, temperature, downward solar and longwave radiation, surface wind speed, specific humidity, and air pressure from a recently updated and improved historical forcing dataset described in Qian et al. (2006). The first 10 yr are devoted to spinup of soil moisture and soil temperature and the remaining 5 yr are used to form climatological annual and seasonal averages of key model diagnostics. Annual global mean results from the sequential experiments described below are cataloged in Table 1.

a. Canopy interception

Clearly, the most egregious bias in ET partitioning is the excessively large contribution from E_C. A high canopy interception rate and high E_C means that much of the atmospheric demand for evaporation is satisfied by E_C, thereby limiting transpiration. Furthermore, in CLM3 plants can only transpire from the dry portion of the canopy, which tends to be a very small part of the canopy during and following a rain event. The canopy interception rate q_{intr} in CLM3 is defined as

$$q_{\text{intr}} = \alpha_l(q_{\text{rain}} + q_{\text{sno}})\{1 - \exp[-0.5(\text{LAI} + \text{SAI})]\}, \quad (1)$$

TABLE 1. Global and annual mean ET and runoff for each of the series of experiments described in section 3. Also shown are two independent estimates of ET partitioning. Global observed runoff estimates are 0.82 mm day^{-1} (Fekete et al. 2002). Q_{SURF} is surface runoff, Q_{DRAIN} is drainage or subsurface runoff, and Q_{TOT} includes runoff from glaciers, wetlands, and lakes as well as surface and subsurface runoff.

Experiment	E_T (%, mm day^{-1})	E_S (%, mm day^{-1})	E_C (%, mm day^{-1})	ET (mm day^{-1})	Q_{SURF} (mm day^{-1})	Q_{DRAIN} (mm day^{-1})	Q_{TOT} (mm day^{-1})
GSWP2 (Dirmeyer et al. 2005)	48, 0.64	36, 0.48	16, 0.22	1.34	0.32	0.63	0.95
Choudhury et al. (1998)	52, —	28, —	20, —	—	—	—	—
CONTROL$_{off}$	13, 0.17	44, 0.57	43, 0.56	1.31	0.34	0.28	0.74
+ Canopy interception reduced	25, 0.27	56, 0.62	18, 0.20	1.09	0.45	0.39	0.95
+ Two-leaf model	28, 0.32	55, 0.64	18, 0.20	1.16	0.44	0.34	0.89
+ Soil water availability to LSM β_t	33, 0.38	50, 0.58	17, 0.20	1.16	0.38	0.25	0.88
+ Soil evaporation beneath canopy reduced (VEG$_{off}$)	38, 0.44	44, 0.51	18, 0.20	1.15	0.43	0.34	0.89
+ Soil hydrology (VEGHYD$_{off}$)	41, 0.52	42, 0.53	17, 0.21	1.27	0.30	0.35	0.77
+ New LAI	44, 0.56	39, 0.50	17, 0.22	1.29	0.28	0.35	0.75

where q_{rain} and q_{sno} are the incident rain- and snow water rates, LAI and SAI are the leaf and stem area indexes, and α_l is a scaling factor that reflects the total fractional area of a leaf that collects water. We reduce canopy interception, and therefore canopy evaporation, by reducing the tuning parameter α from 1.0 to 0.25, a value that more realistically reflects that only one side of a leaf can collect water and that rainwater tends to bead on the leaf and does not typically wet the entire exposed leaf surface. Global mean E_C drops to 18% of total ET while E_T increases to 25% and E_S rises to 56% following this change (Table 1).

b. Two-leaf model

A new model for canopy integration, developed in Thornton and Zimmerman (2007), is introduced in which canopy leaf area is decomposed into two fractions, sunlit and shaded. While the shaded portion of the canopy is essentially inactive in CLM3, in the new model, shaded leaves receive a fraction of the diffuse radiation and are therefore permitted to photosynthesize and transpire, although at a lower rate than the sunlit portion of the leaves. This modification represents an obvious improvement in the physical realism of the model and significantly increases canopy transpiration rates. The transpiration E_T rises slightly following this change (Table 1).

c. Soil water availability

The soil water availability factor (β_t) relates soil moisture conditions to soil moisture stress on plant photosynthesis and transpiration. The factor β_t is a function of soil water matric potential and root distribution and ranges between 0 (at wilting point potential) and 1 (at saturated soil matric potential) (Oleson et al. 2004). All other factors being equal, low values of β_t act to decrease the rate of photosynthesis, stomatal conductance, and E_T. Here, we revert from the CLM3 parameterization of soil water availability to that of the National Center for Atmospheric Research Land Surface Model (NCAR LSM), which ranges linearly with soil water from wilting point ($\beta_t = 0$) to maximum ($\beta_t = 1$) (Bonan 1996). For particular soil moisture conditions, the LSM representation yields β_t values that are greater than or equal to that using the standard CLM3 representation, a difference that increases with drier soils (Bonan et al. 2002). This change effectively permits plants to more readily access soil water and leads to a global mean increase in β_t of about 0.05, which contributes to a further rise in E_T to 33% of total ET (Table 1).

d. Soil evaporation from beneath a canopy

Although the alterations introduced to this point improve ET partitioning, the fraction derived from E_S remains high. On the global scale, high E_S relative to E_T may be related to CLM3's dry bias in deep soil layers, which results in high soil moisture stress, even in regions where heavy rainfall should provide ample water for transpiration, for example, in the southeastern United States and Amazonia. Improvements to CLM3 soil hydrology are addressed below. The high E_S contribution relative to E_T, however, cannot fully be attributed to the dry soil bias. Figure 2 shows $E_T/(E_T + E_S)$

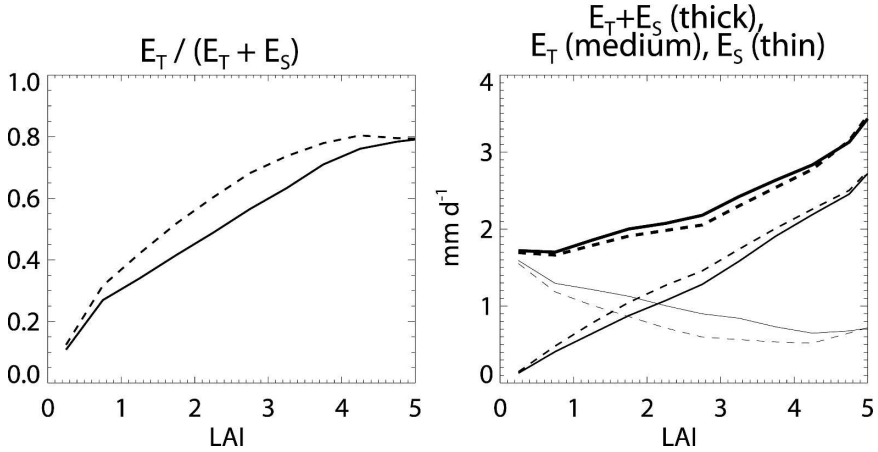

FIG. 2. (left) LAI vs $E_T/(E_T + E_S)$ and (right) LAI vs E_T, E_S, and $E_T + E_S$ for the offline CLM3 experiment with reduced interception, the two-leaf model, and using LSM β_t (solid lines) and the offline CLM3 experiment with these changes plus the parameter changes to C_S described in the text (dashed lines). Plots are constructed by identifying all days where E_C is less than 0.1 mm and β_t is greater than 0.8 (e.g., days where canopy water does not restrict E_T and soils are wet) and then binning and averaging E_T and E_S on these days according to grid box mean LAI. All nonice land grid points are considered to create the binned averages.

as a function of LAI for saturated soil conditions for a simulation that includes all the modifications introduced to this point. The relationship between $E_T/(E_T + E_S)$ and LAI is nearly linear. Here E_T accounts for 50% of $E_T + E_S$ at LAI $\approx$ 2.5 and reaches 80% at LAI $\approx$ 5. This behavior is in contrast with that found by Schulze et al. (1994), who show that the $E_T/(E_T + E_S)$ versus LAI relationship is nonlinear with the contribution from E_T rising sharply at low LAI, hitting 50% at LAI $\approx$ 1, before reaching around 90% at LAI $\approx$ 5. The discrepancy between the Schulze et al. analysis and CLM3 behavior suggests that E_S from beneath a canopy is excessive in CLM3. This interpretation is supported, for example, by observations at an aspen forest site in Saskatchewan, Canada, where only 5% of annual ET comes from soil evaporation (Black et al. 1996).

The relative contribution of E_T and E_S in vegetated regions can be altered by adjusting two parameters in the equation for the turbulent transfer coefficient between the soil and the canopy air (C_S). In CLM3, C_S is defined as (Zeng et al. 2005)

$$C_S = C_{S,\text{bare}}W + C_{S,\text{dense}}(1 - W), \quad (2)$$

where the weight W is

$$W = e^{-\alpha(\text{LAI}+\text{SAI})}, \quad (3)$$

$C_{s,\text{bare}}$ is the turbulent transfer coefficient for bare soil and is a function of the wind velocity incident on the leaves, $C_{s,\text{dense}} = 0.004$ and is the value used in CLM3 for a dense canopy, and α is set to 1 in CLM3. This formulation for the turbulent transfer coefficient calculation is derived in Zeng et al. (2005) and was motivated by the need to reduce a large CLM2 surface air temperature bias seen in low-LAI, semiarid regions. Here, we adjust $C_{s,\text{dense}}$ to 0.0025 and α to 2, parameter values that generate an $E_T/(E_T + E_S)$ versus LAI relationship that is in better agreement with Schulze et al., further improving global ET partitioning by reducing E_S (38% E_T, 44% E_S, and 18% E_C; Table 1) while maintaining reasonable surface air temperatures. Note that we tested with a number of parameter values for $C_{s,\text{dense}}$ and α. Although somewhat larger changes to these parameters result in a better agreement with Schulze et al., they also generate undesirably large changes in surface air temperature.

e. Soil hydrology

The preceding changes to the model significantly improve the partitioning of ET, but global fractional E_T remains low compared to other model estimates. CLM3 is characterized by dry deep soil layers and a small amplitude soil moisture annual cycle that result in excessive soil moisture stress on transpiration, especially during "dry" seasons. This unrealistic behavior is illustrated in Fig. 3, which shows mean Amazon basin annual cycle time series for a number of hydrologic cycle quantities for the $\text{CONTROL}_{\text{off}}$ run and a simulation that includes all the changes introduced to this point, hereafter referred to as VEG_{off} for vegetation scheme-related changes (note that results from the experiment $\text{VEGHYD}_{\text{off}}$ that are also shown in Fig. 3 are described and discussed below). Observational and model esti-

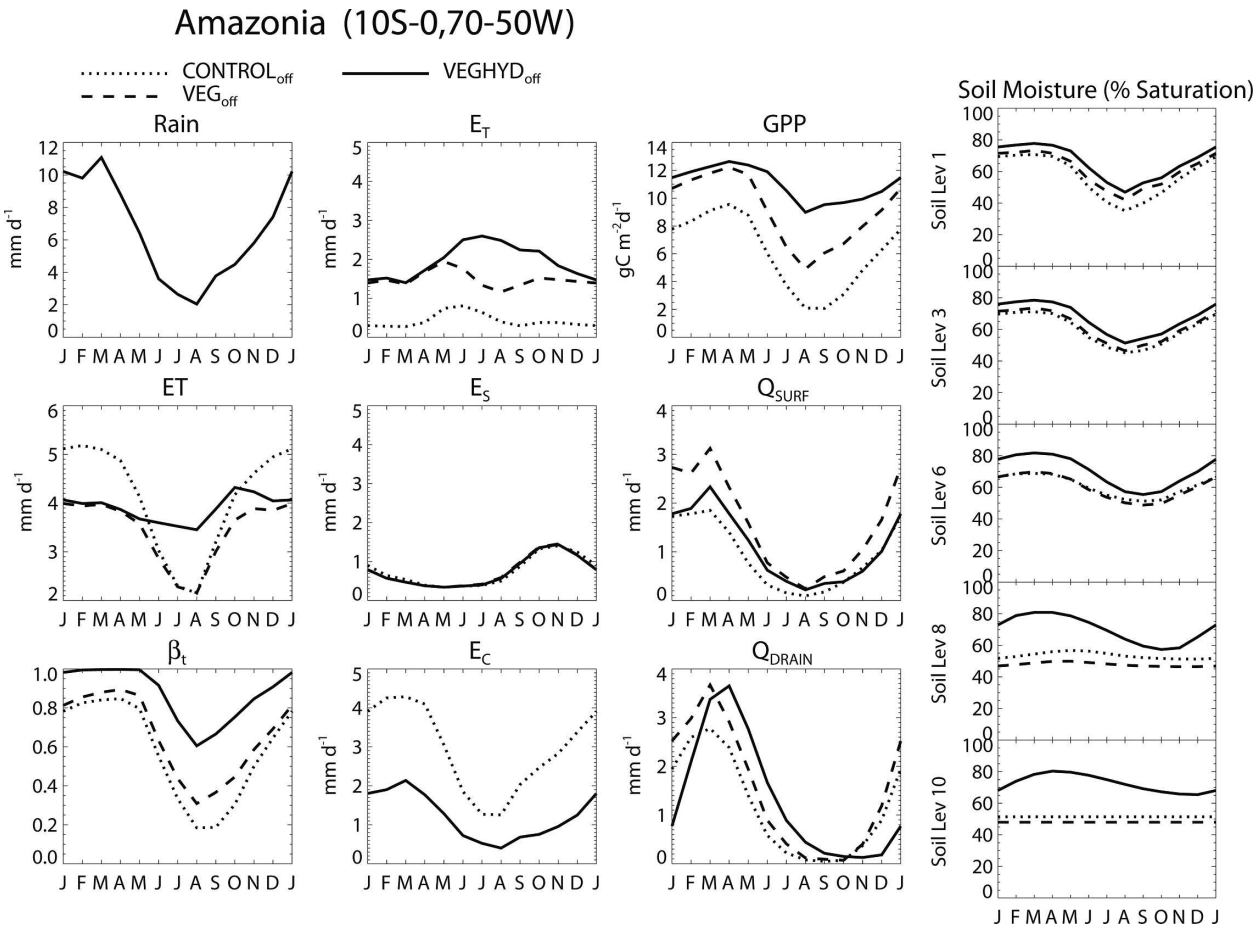

FIG. 3. Mean annual cycle of components of the hydrologic cycle for CONTROL$_{off}$, VEG$_{off}$, and VEGHYD$_{off}$ experiments. Q_{SURF} is surface runoff, Q_{DRAIN} is drainage. GPP is gross primary production.

mates indicate that the ET annual cycle in the Amazon basin is relatively flat, with slightly higher values seen during the wet season and slightly lower values seen toward the end of the dry season but not varying substantially across the year (Nobre et al. 1996; Malhi et al. 2002; Werth and Avissar 2004). The ET annual cycle in CONTROL$_{off}$ exhibits what appears to be an unrealistically large annual cycle. High ET during the rainy season is reduced in VEG$_{off}$ due to a reduction in E_C that is not fully compensated for by increased E_T. In both simulations, the small soil moisture store is quickly depleted, leading to high soil moisture stress on E_T and low total ET and photosynthesis from June to September. Shuttleworth (1988) finds that E_T actually increases during the dry season, with plants drawing on large soil moisture stores that swell during the rainy season and making use of the high incoming solar radiation associated with low dry-season cloud cover. The biases described here are accentuated in the coupled model because of a deficit in precipitation compared to observations.

After a series of tests, the following modifications were introduced that together combine to moisten deep CLM3 soils and increase interseasonal soil moisture storage, while maintaining a reasonable runoff simulation:

- CLM3 subsurface runoff is the sum of lateral drainage from soil layers 6–9 and drainage out through the bottom of the soil column. Lateral drainage is very efficient in CLM3, leading to a dry and unvarying bottom soil layer and rapid flushing of soil water out of the column, which suppresses interseasonal soil water storage. This flow out of the grid cell is directed into runoff rather than to an adjoining cell so the soil water is effectively lost from the soil. Here, lateral drainage is turned off, which permits greater soil moisture filtration into the bottom layer and enhances interseasonal soil moisture storage.
- VEG$_{off}$ has more total runoff compared to CONTROL$_{off}$ (see Table 1 and Fig. 3), partly because substantially more rain and dripfall reaches the soil surface due to

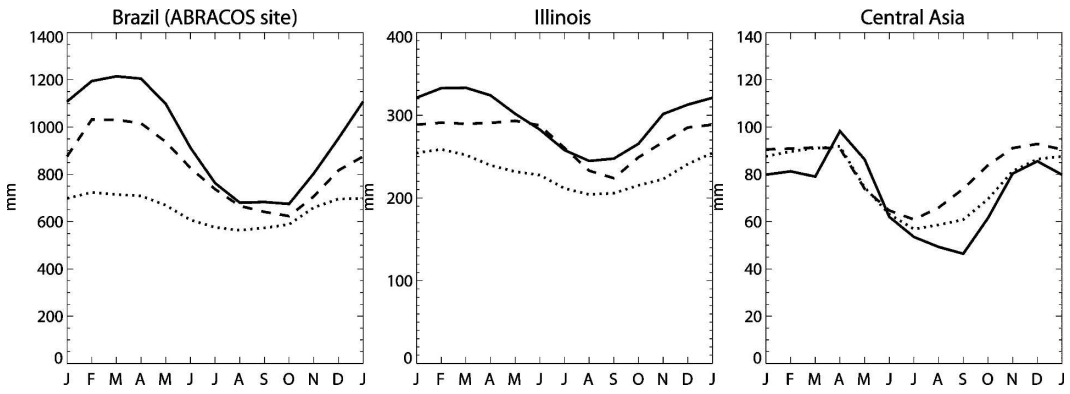

FIG. 4. Observed (solid) and modeled ($CONTROL_{off}$, dotted; $VEGHYD_{off}$, dashed) mean annual cycles of soil moisture. For ABRACOS tower site (10°S, 61.5°W) model results are from 1D CLM3 forced with tower site data for the period 1992–93. Illinois and central Asia observed data are multilocation mean [19 stations and averaged as in Dai et al. (2004)] representing 37°–44°N, 86°–94°W and 50°–55°N, 70°–100°E, respectively. Model data for Illinois and central Asia are averaged over corresponding regions. Model soil moisture content is integrated down to 3.43-, 0.9-, and 1.0-m depth for ABRACOS, Illinois, and central Asia, respectively.

the reduction in canopy interception. Consequently, significantly more incident water is directed into surface runoff in VEG_{off} (21% globally, 22% Amazon) compared to $CONTROL_{off}$ (16.5% globally, 14% Amazon). The increase in surface runoff, particularly in the Amazon region is undesirable as observations suggest that there is very little surface runoff even after heavy precipitation (Hodnett et al. 1996). To encourage infiltration of water into the soil column, we introduce an infiltration enhancement factor, similar to that used in the Met Office Surface Exchange Scheme (Essery et al. 2001) for the unsaturated fraction of the grid box. The enhancement factor is derived from the weighted mean of root density in the top three soil layers and is meant to represent water conduits into the soil provided by roots. Note that an alternative way to increase infiltration is through a two-mode soil pore size distribution that permits the representation of soil macropores (Liu and Dickinson 2003). This formulation also enhances infiltration but requires a new global surface dataset for soil particle size distribution. For the sake of simplicity, the infiltration enhancement factor is used here.

- Saturated hydraulic conductivity (K_{sat}) contains a scaling factor in CLM3 that generates an exponential decrease in K_{sat} with soil depth that reflects the decrease in permeability at deeper soil levels (Beven 1984; Elsenbeer et al. 1992). However, this vertical variation in K_{sat} is accounted for explicitly in CLM3 as vertical variations in soil texture incorporated into the soil dataset (increasing clay content with depth). To eliminate this "double counting" of the vertical variation of K_{sat}, the exponential scaling factor for K_{sat} is removed.

Offline tests of the modifications to soil hydrology (hereafter $VEGHYD_{off}$ for all vegetation and hydrology modifications) show a significant impact on soil wetness, runoff, and ET partitioning. Globally, soils are considerably wetter, especially at deep soil levels, and the annual cycle of soil moisture is far more pronounced in most areas. Figure 4 shows observed annual cycles of soil moisture for the Anglo-Brazilian Amazonian Climate Observation Study (ABRACOS) site in Rondônia, Brazil (Gash et al. 1996); station data averaged over 19 sites in Illinois (Hollinger and Isard 1994); and station data averaged over 11 sites in central Asia (Vinnikov and Yeserkepova 1991). The latter two datasets were obtained from the Global Soil Moisture Data Bank (Robock et al. 2000). For both ABRACOS and Illinois, the new hydrology parameterizations result in both better mean soil moisture and, more notably, an improved representation of the annual cycle. The impact in the semiarid climate of central Asia is minimal.

Wetter root-zone soil moisture contributes to an increase in global E_T (41% E_T, 42% E_S, and 17% E_C; Table 1). Total ET is only slightly lower in $VEGHYD_{off}$ (1.27 mm day^{-1}) compared to $CONTROL_{off}$ (1.31 mm day^{-1}). There is a corresponding increase in total runoff; an increase that is in the right direction as $CONTROL_{off}$ has a small negative bias in mean annual total runoff compared to the Fekete et al. (2002) runoff climatology. The global runoff ratios (runoff divided by precipitation) for Fekete, $CONTROL_{off}$, and

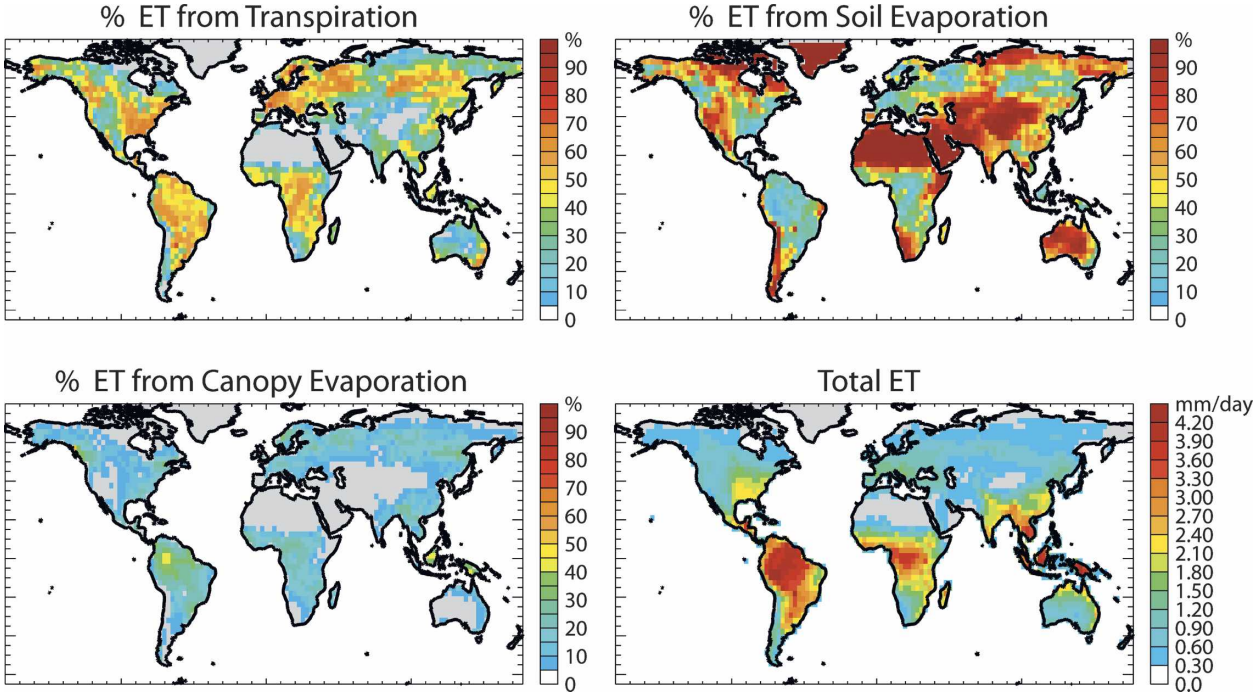

FIG. 5. Same as in Fig. 1, but for $\text{VEGHYD}_{\text{off}}$.

$\text{VEGHYD}_{\text{off}}$ are 0.40, 0.36, and 0.38, respectively. This bias is also apparent in long-term mean global river discharge. Dai and Trenberth (2002) estimate river discharge to be 1.20×10^6 m^3 s^{-1}, while $\text{CONTROL}_{\text{off}}$ and $\text{VEGHYD}_{\text{off}}$ produce discharges of 1.08 and 1.15×10^6 m^3 s^{-1}.

The impact of the hydrology modifications varies regionally but can be summarized by their impact in Amazonia (see Fig. 3). The clearest impact is that the deep soil levels now accumulate moisture throughout the wet season, which permits plants to transpire throughout the dry season, drawing on the stores of moisture accumulated during the wet season. Because of the increase in dry-season E_T, total ET is much less variable over the course of the year, as desired. Note also that while surface runoff is higher in VEG_{off}, the infiltration enhancement factor brings it back down in $\text{VEGHYD}_{\text{off}}$, thus permitting more incident water to enter the soil.

The global ET partitioning in $\text{VEGHYD}_{\text{off}}$ is shown in Fig. 5. The partitioning (41% E_T, 42% E_S, and 17% E_C) is in much better agreement with prior estimates, although E_T remains somewhat low and E_S a little high compared to other estimates. An improved CLM3 surface dataset based on Moderate Resolution Imaging Spectroradiometer (MODIS) data became available during the latter stages of this study, which significantly alters prescribed LAI (P. Lawrence 2005, personal communication). In the new dataset many regions, such as the tropical rain forests and South Asia, are characterized by notably higher LAI, while in predominantly agricultural regions, such as the eastern United States and Europe, the shift is toward smaller LAI. When $\text{VEGHYD}_{\text{off}}$ is run with the new CLM3 surface dataset, ET partitioning is further improved (44% E_T, 39% E_S, and 17% E_C).

Overall, ET partitioning in $\text{VEGHYD}_{\text{off}}$ is more in line with what one would intuitively expect with E_T dominant in tropical rain forest and heavy agricultural regions, while E_S is a more significant component of ET in arid and semiarid regions. The canopy evaporation E_C is much reduced globally but remains a significant component of total ET in areas with dense canopies, such as the Amazon and central Africa. The large shift in ET partitioning is particularly apparent in Amazonia where partitioning shifts from 11% E_T, 18% E_S, and 71% E_C in $\text{CONTROL}_{\text{off}}$ to 51% E_T, 19% E_S, and 30% E_C (58% E_T, 9% E_S, and 33% E_C with the new LAI dataset) in $\text{VEGHYD}_{\text{off}}$.

4. Impact of ET partitioning on climate simulations

a. *Mean climate*

In this section, the impact of the imposed changes to CLM3 on the CAM3–CLM3 climate is evaluated.

TABLE 2. Annual mean properties of CAM3–CLM3 CONTROL and VEGHYD simulations averaged over all land points.

Variable	CAM3–CLM3 CONTROL	CAM3–CLM3 VEGHYD
Precipitation (mm day^{-1})	2.31	2.37
2-m temperature (K)	282.6	282.3
Latent heat (W m^{-2})	42.0	45.5
Sensible heat (W m^{-2})	29.8	26.0
Transpiration (%, mm day^{-1})	11, 0.16	33 (42), 0.52
Soil evaporation (%, mm day^{-1})	57, 0.82	54 (41), 0.84
Canopy evaporation (%, mm day^{-1})	32, 0.46	13 (17), 0.21
Total evapotranspiration (mm day^{-1})	1.44	1.57
Surface runoff (mm day^{-1})	0.432	0.340
Subsurface runoff (mm day^{-1})	0.365	0.396
Incoming solar (W m^{-2})	179.3	175.9
Absorbed solar (W m^{-2})	135.0	132.6
Incoming longwave (W m^{-2})	311.5	312.3
Emitted longwave (W m^{-2})	374.2	372.7
Net radiation (W m^{-2})	72.4	72.1
Photosynthesis (GPP, Pg C yr^{-1})	65	148
Soil moisture stress (B_t)	0.35	0.51
Soil moisture (mm)	301	342

The CONTROL and VEGHYD versions of the model are run for 22 yr (1979–2000), forced by observed sea surface temperatures and initialized with a spunup land surface state derived from the respective offline experiments. Only the last 17 yr are analyzed to allow the model to adjust to the initial conditions. Table 2 lists annual mean values, averaged over all land points, for the CONTROL and VEGHYD experiments. ET partitioning is improved from 11% E_T, 57% E_S, and 32% E_C in CONTROL to 33% E_T, 54% E_S, and 13% E_C in VEGHYD. The improvement is less than that seen in the offline experiments. To a certain extent, the difference in ET partitioning between the CAM3–CLM3 coupled and CLM3 offline experiments is related to biases in CAM3–CLM3 precipitation, biases that are essentially unaffected by the CLM3 VEGHYD changes. These include a deficit of precipitation in some heavily forested areas, where E_T should dominate but does not, such as the southeastern United States and Amazonia, and significant overestimates of precipitation in semiarid and arid regions, where E_S contributes significantly, particularly in Saudi Arabia and India (Hack et al. 2006). If one considers only locations where CAM3 annual mean precipitation is within 20% of the Global Precipitation Climatology Project (GPCP; Adler et al. 2003) observed precipitation estimates, the ET partitioning is similar to that of the offline model (42% E_T, 41% E_S, and 17% E_C).

There are some additional broad changes to climate seen in VEGHYD, apart from ET partitioning. For example, the global hydrologic cycle is slightly more vigorous with modest increases seen in both global precipitation (2.31 to 2.37 mm day^{-1}; GPCP estimate, 2.15 mm day^{-1}) and ET (1.44 to 1.57 mm day^{-1}) while runoff decreases (0.86 to 0.80 mm day^{-1}). The increase in precipitation may reflect the global mean 3 W m^{-2} redistribution of surface available energy into latent heat flux at the expense of sensible heat flux, a redistribution that is likely driven by the overall wetter soils. On average, global soil water storage rises by 13%, an increase that corresponds to a more substantial 46% increase in global mean β_t (0.35 to 0.51). Photosynthesis, or gross primary production (GPP), also increases substantially from 64 to 148 Pg C yr^{-1}, which compares reasonably with global estimates of around 120 Pg C yr^{-1} (Schlesinger 1997), especially when one considers that nitrogen limitation on photosynthesis is not yet incorporated into CLM.

The changes to model climate exhibit significant regionality. Seasonal mean maps of VEGHYD minus CONTROL differences in precipitation, temperature, ET, runoff, β_t, and photosynthesis are shown for June–August (JJA; Fig. 6) and December–February (DJF; Fig. 7). Of initial concern is whether or not the modifications improve or degrade the overall climate simulation. The impacts on precipitation cannot be classified clearly as an improvement or degradation of the model precipitation climatology, although the increase in summer precipitation in the southeastern United States is an improvement. The impacts on temperature, however, broadly drive the model toward improved agreement with the observations (Willmott and Matsuura 2000). In particular, higher ET in the Northern Hemisphere midlatitudes (30°–50°N) and Amazonia contributes to a reduction in JJA warm biases. Similarly, higher dry-season E_T contributes to a reduction of a significant DJF warm bias in India.

The reduction seen in JJA runoff over southern Asia and Alaska (see Fig. 6) is related to an approximately 1-month delay in the timing of peak runoff as soil water is forced in VEGHYD to percolate through the entire column before exiting the bottom of the soil column. In India, for example, runoff peaks during JJA in CONTROL but peaks during July–September in VEGHYD, leading to the reduced JJA runoff seen in Fig. 6. This effect occurs in Southeast Asia as well, but with additional reduction in runoff related to enhanced E_T during DJF that is not balanced by increased precipitation.

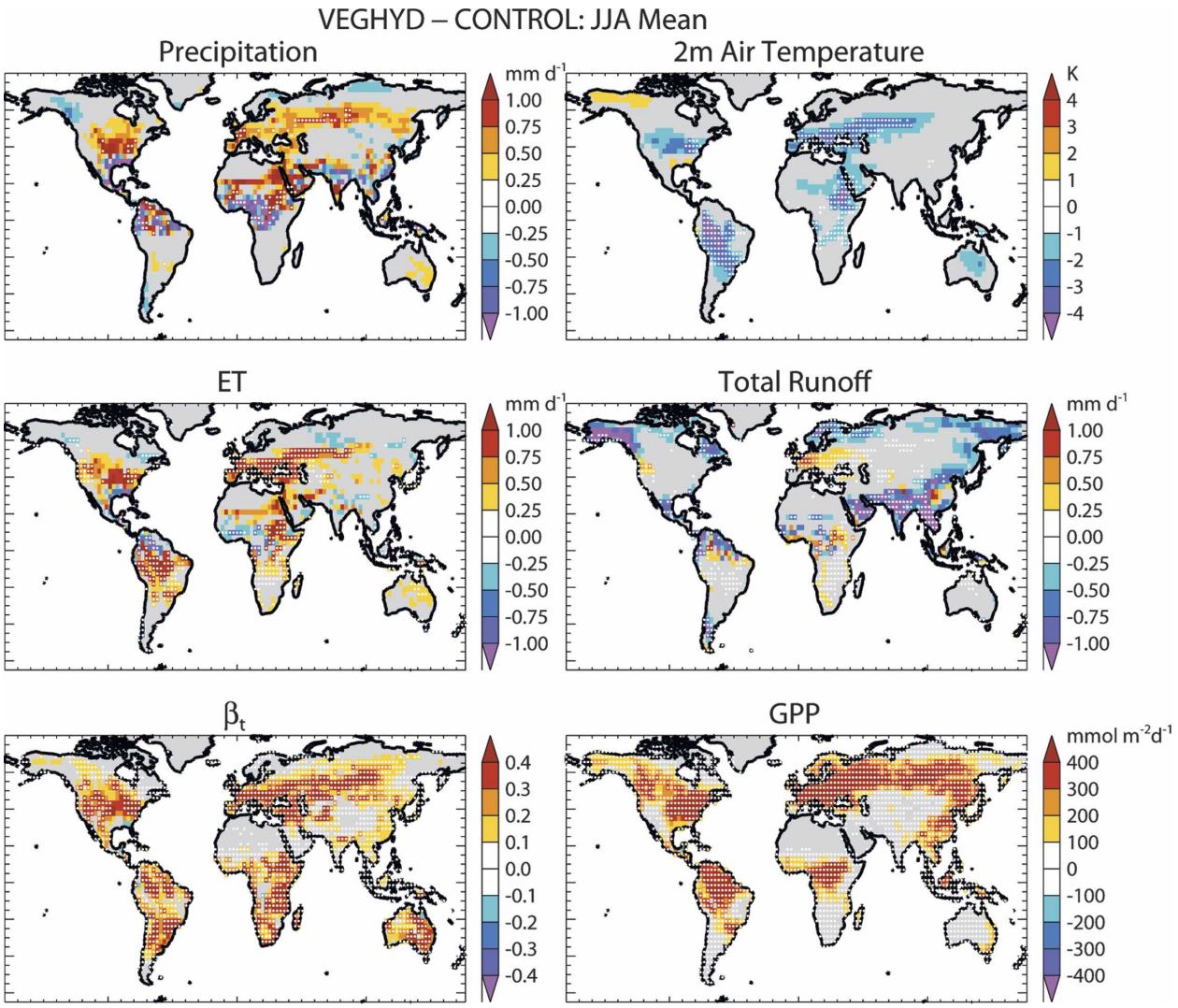

FIG. 6. Global maps of differences in JJA means between CAM3–CLM3 VEGHYD and CONTROL experiments for selected diagnostics. Stippling indicates that local difference passes the Student's *t* test for statistical significance of differences in means at 95% confidence level.

b. Soil water storage and soil moisture memory

Overall, soils are wetter throughout the year in most locations, except in very high latitude and arid regions. The factor β_t is correspondingly higher across the same regions, as is photosynthesis. Wetter soils correspond to greater soil water storage, which in turn permits plants to continue to transpire during dry periods. This transformation in model behavior is emphasized in Fig. 8, which shows, for CONTROL and VEGHYD, the average number of months during the year when evapotranspiration exceeds precipitation ($P - ET < 0$). In CONTROL, ET rarely exceeds precipitation, suggesting that typically precipitation is rapidly recycled as ET or lost from the soil column through runoff. In contrast, VEGHYD exhibits numerous grid points where $P - ET < 0$ for more than 3 month yr^{-1}.

Does this change in $P - ET$ behavior indicate longer soil moisture memory time scales in VEGHYD? Not necessarily: it may simply reflect higher mean soil moisture values. It is interesting, nonetheless to consider how the hydrology modifications affect time scales of soil moisture memory. Figure 9 shows maps and vertical profiles averaged over a number of latitude bands of the lag-one autocorrelation coefficient, a single parameter measure of soil moisture memory (Wu and Dickinson 2004). For each grid point and soil layer, the anomaly time series of volumetric soil water is correlated with itself but lagged by one month. The anomaly time series is generated by subtracting the climatologi-

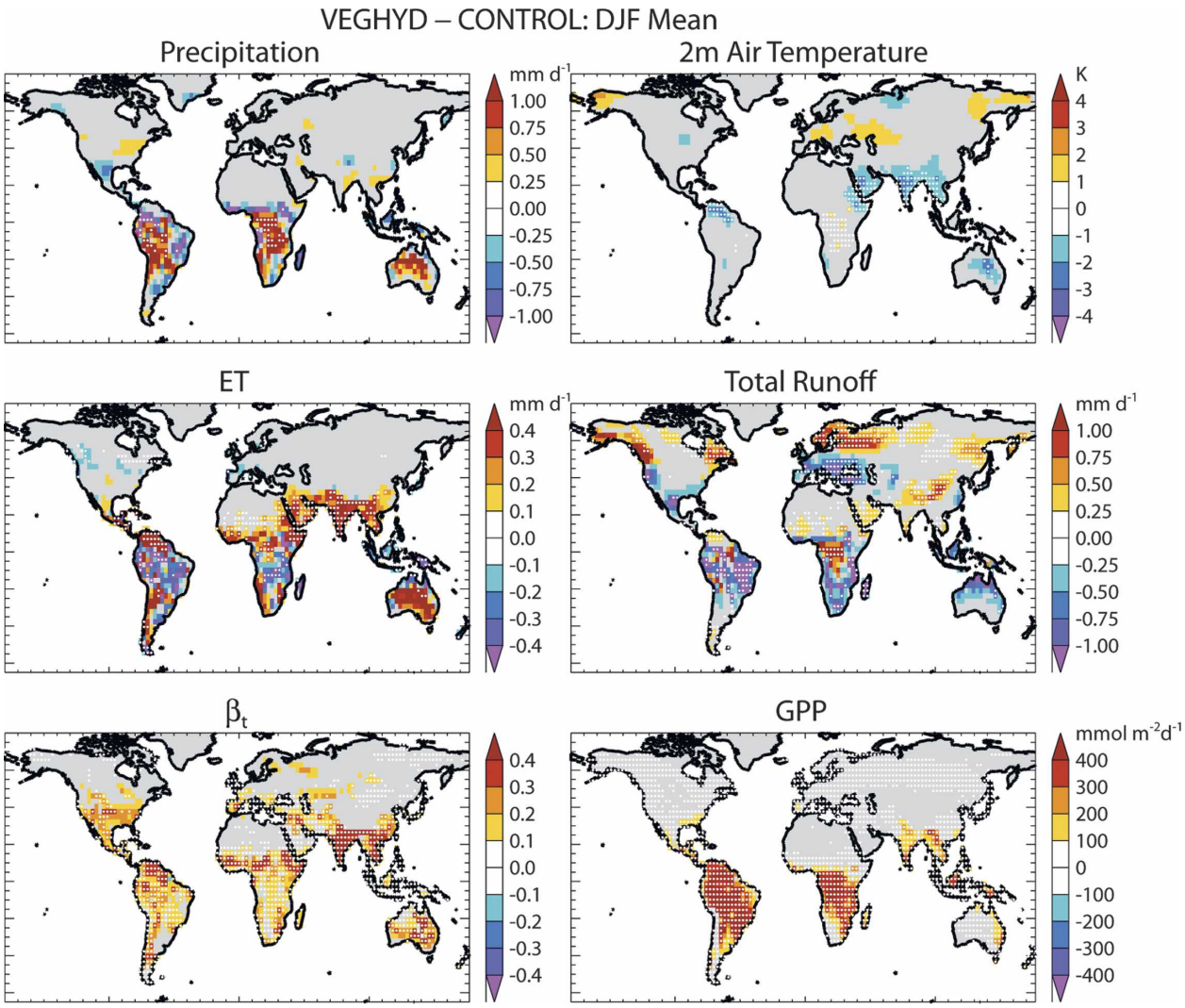

FIG. 7. Same as in Fig. 6, but for DJF.

cal mean annual cycle from the monthly mean time series. Higher autocorrelation values indicate longer anomaly decay time scales; autocorrelations of 0.8, 0.6, 0.4, and 0.2 correspond to *e*-folding anomaly decay time scales of 4.5, 2.0, 1.1, and 0.6 months, respectively (Wu and Dickinson 2004). For the most part, differences in soil moisture memory between CONTROL and VEGHYD can be attributed to the impacts of the model modifications to ET, the partitioning of incident precipitation into infiltration and runoff, and the rate at which water percolates through (and out of) the soil column. However, soil moisture memory, as discussed in Koster and Suarez (2001), also depends on the seasonality in the statistics of atmospheric forcing and the strength of the land–atmosphere feedback. While the contribution of changes in these influences across the two models cannot fully be discounted, it is reasonable to expect that the direct changes to model parameterizations are more likely responsible for the soil moisture memory differences seen than the more subtle changes to model climate.

CONTROL and VEGHYD exhibit significant differences in the vertical profile of the lag-one autocorrelation with depth. In general, soil moisture autocorrelations increase with soil depth. In the uppermost part of the soil column, the time scale of soil moisture persistence is low due to the influence of strong precipitation and evaporation forcing from above, whereas deeper in the soil column, a soil moisture anomaly can persist for many months and is set more strongly by the rate at which water permeates through the soil column. Below about 0.5-m depth soil moisture persistence is considerably shortened in VEGHYD. This reduction in soil moisture memory deep in the soil is related to the en-

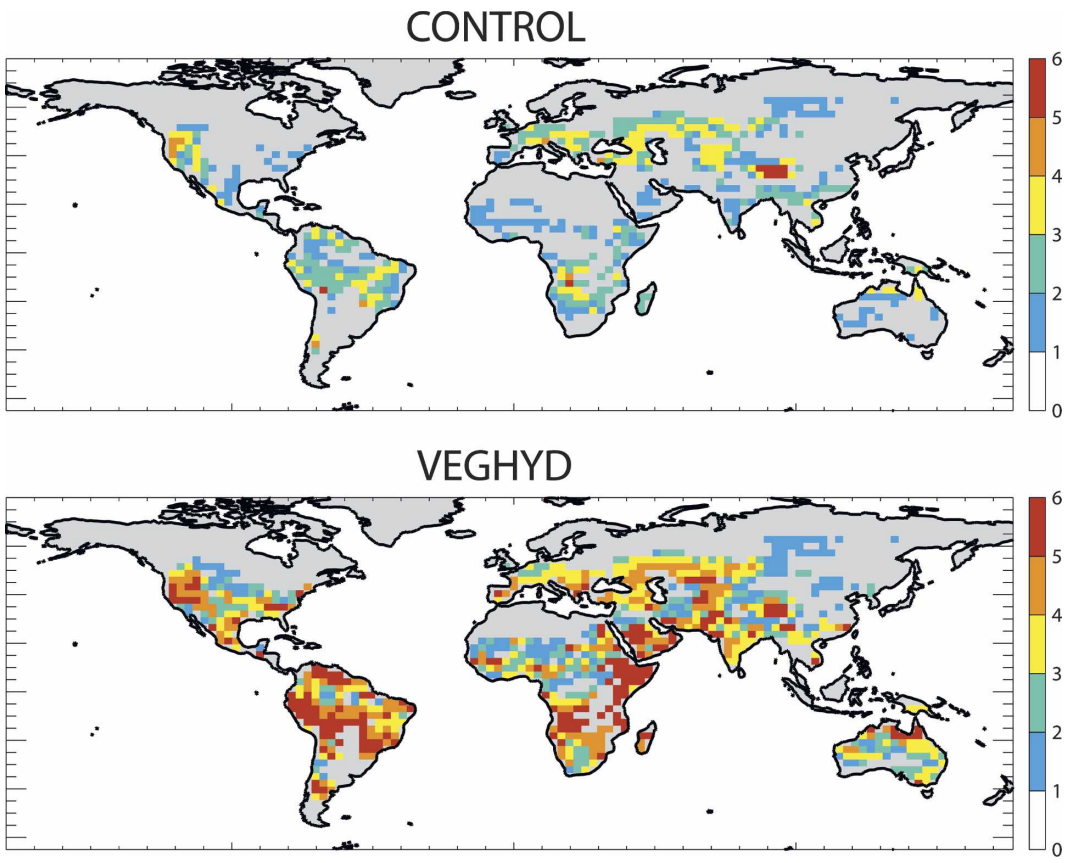

FIG. 8. Global maps showing number of months during the year when evapotranspiration exceeds precipitation ($P - \mathrm{ET} < 0$). Grid points with lake or wetland fractional coverage exceeding 50% are not considered.

hanced soil moisture annual cycle in VEGHYD. In CONTROL, the efficient export of soil water out of the soil column as midlevel drainage prevents the deepest soil layers from experiencing much soil moisture variation on annual time scales. The relative constancy corresponds to high lag-one autocorrelation values and extended soil moisture memory time scales. Even though the diagnosed time scales are lengthy in CONTROL, the actual soil moisture anomalies are very small and are not felt by the atmosphere despite persisting for long periods. In contrast, interannual variability at depth is considerably higher in VEGHYD than in CONTROL (not shown). Therefore, even though the soil moisture anomaly persistence time scales are shorter, due to more rapid loss of water through transpiration and faster percolation of water through the soil column, an anomaly that develops is far more likely in VEGHYD to exert a detectable influence on subsequent seasons' climate.

c. *Response to rain event*

The shift in how CLM3 partitions ET is likely to affect the turbulent flux and temperature responses to a precipitation event, which can, in turn, influence land–atmosphere feedbacks. A priori, one would expect that in CONTROL the high interception and soil evaporation would lead to a sharp increase in ET directly following a rain event, with ET dropping off quickly after the canopy water store is exhausted. On the other hand, since E_T is more important in VEGHYD, one would anticipate the ET response to a rain event in VEGHYD to be slightly delayed relative to the precipitation event and to extend for a longer time period. This behavior is precisely what is seen in composites of the 5-day evolution of ET and temperature subsequent to a heavy rain event. We calculate lagged composites of ET and temperature relative to rain events that meet the following conditions: (i) rain exceeds 5 mm day^{-1}, and (ii) event is followed by five consecutive days with rainfall rates less than 0.5 mm day^{-1}. A total of 16-yr of daily JJA data from CONTROL and VEGHYD are considered for the composites. Results are shown for two regions, both of which are characterized by strong shifts in ET partitioning: the eastern United States (Fig. 10) and Amazonia (Fig. 11). By coincidence rather than design, the day −2 to day 0 precipitation composites are

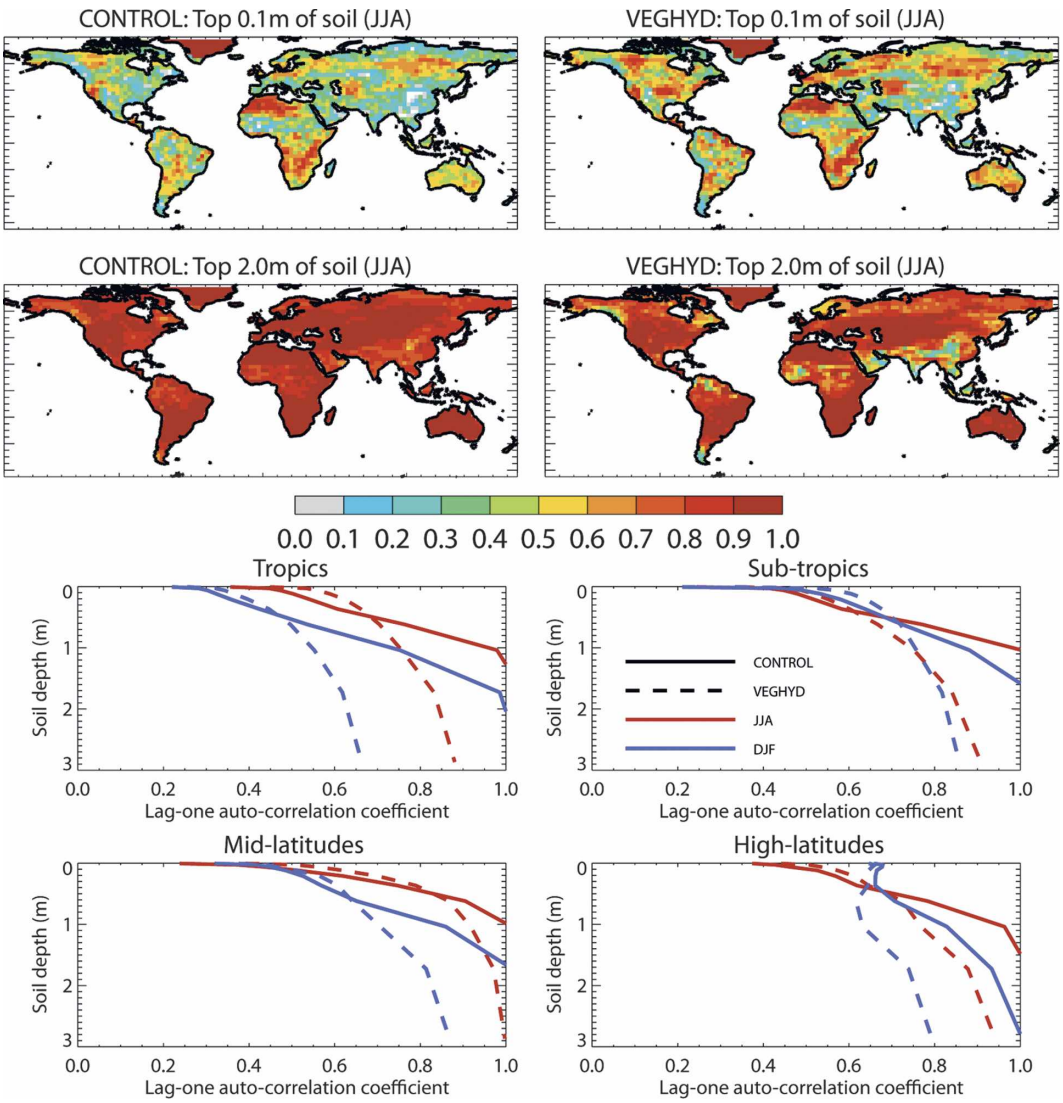

FIG. 9. The average of soil moisture 1-month-lag autocorrelation for JJA for (upper maps) top 0.1 m of soil and (lower maps) top 2.0 m of soil for CONTROL and VEGHYD. Latitude belt mean lag-one autocorrelation coefficients vs soil depth for JJA and DJF in CONTROL and VEGHYD. Latitude belts are Tropics (14°S–14°N), northern subtropics (14°–33°N), northern midlatitudes (33°–56°N), and northern high latitudes (56°–73°N).

nearly identical in CONTROL and VEGHYD. Considering first the eastern U.S. composites, ET peaks on day 0 in both CONTROL and VEGHYD, but the peak is lower in VEGHYD due to the smaller E_C contribution on the same day as the rainfall event. Both E_T and E_S peak on day +1 for both models, but the E_T peak is stronger and the E_S peak is weaker in VEGHYD. ET follows a similar downward trajectory from day +1 to day +5 in CONTROL and VEGHYD, but ET is about 1 mm day^{-1} higher, due mainly to higher E_T, in VEGHYD. The temperature response is consistent with the ET response, with temperatures hitting a minimum on the day of the rainfall event in CONTROL, due to enhanced ET and reduced incident solar radiation due to cloud cover, and recovering quickly in the subsequent days. Persistently high ET after the rain event leads to a delayed temperature recovery in VEGHYD. The composite picture is similar for Amazonia, with the main difference being a more subdued ET response to a rain event in VEGHYD due to the relatively weak mean moisture limitation on ET.

The number of events with rain followed by five consecutive dry days is sharply lower for both focus regions (eastern United States: 369 in CONTROL and 157 in VEGHYD; Amazonia: 412 in CONTROL and 114 in VEGHYD). Mean precipitation, however, is essentially

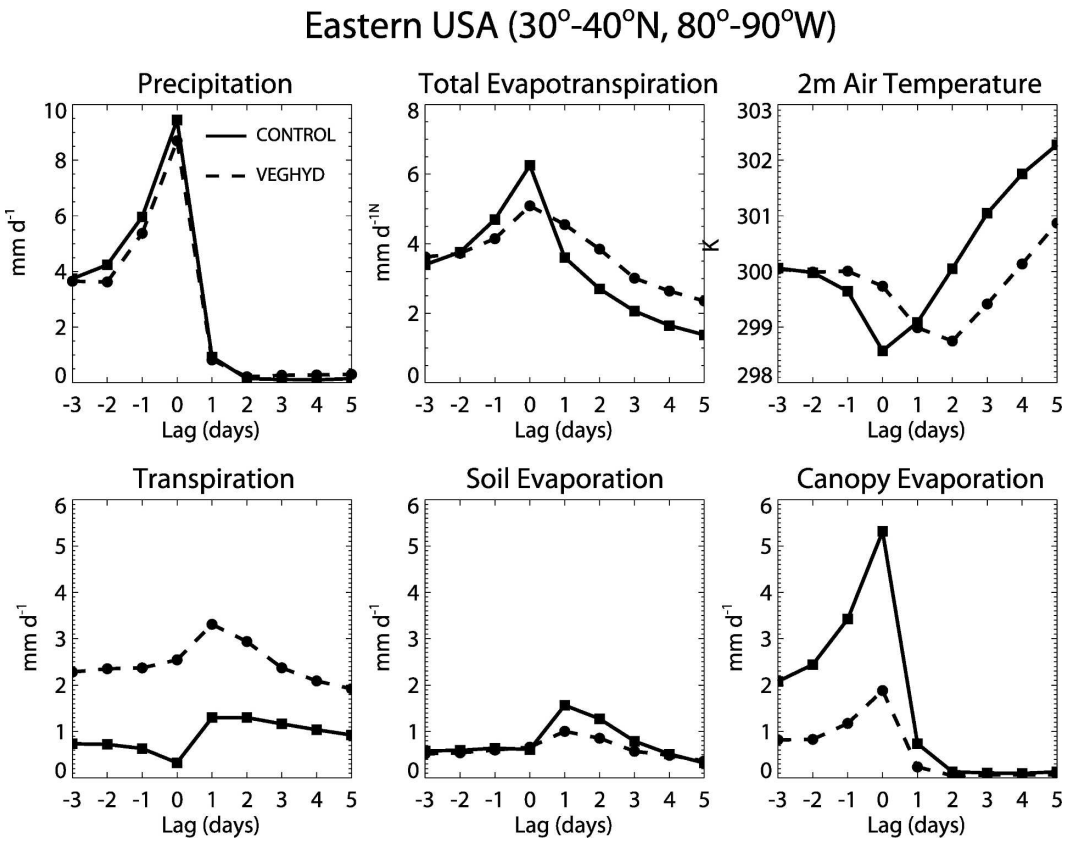

FIG. 10. Composites of the model response in terms of ET and 2-m air temperature to all rainfall events that are followed by five consecutive rain-free days. Events are identified separately for each grid box located within the eastern U.S. region (30°–40°N, 80°–90°W).

unchanged between CONTROL and VEGHYD for both regions. This implies a shift in the precipitation distribution. Figures 12a,b show the JJA precipitation distribution for CONTROL and VEGHYD for the eastern U.S. and Amazonia regions. In both regions, the shift is toward more frequent light rainfall at the expense of heavy rainfall. Intuitively, the shift makes sense, especially when it is considered in the context of the known strong sensitivity of precipitation to surface turbulent heat flux forcing in CAM3–CLM3 (Guo et al. 2006). Due to the steadying influence of transpiration, which responds slowly to longer-term weather anomalies, the day-to-day variability of latent heat flux is lower in VEGHYD compared to CONTROL, in both regions. In the absence of strong forcing associated with large latent heat flux excursions from the norm, precipitation rates remain fairly steady in VEGHYD. A scatter diagram of the change in latent heat flux variability versus the change in the median wet-day rain rate is shown in Fig. 12d [a change in the median wet-day rain rate is a simple way to detect a shift in precipitation distribution; Osborn et al. (2000)]. In general, an increase in latent heat flux variability corresponds to a shift toward more heavy rain events and vice versa, although the correlation coefficient is modest (r = 0.43), indicating that other factors are likely involved. Changes in mean latent heat flux do not, however, correlate with shifts in the precipitation distribution (r = −0.09, Fig. 12c).

d. Global Land–Atmosphere Coupling Experiment

The GLACE model intercomparison (Guo et al. 2006; Koster et al. 2006) demonstrated that the strength of interaction between the land surface and the atmosphere varies widely across current GCMs. CAM3–CLM3 is one of the strongest models in terms of the diagnosed influence of subsurface soil moisture on precipitation even though E_T, the portion of ET that is directly influenced by subsurface soil moisture, is only a small fraction of total ET in CONTROL, the model version used for the GLACE study. It is interesting, therefore, to recalculate land–atmosphere coupling strength for VEGHYD to see whether and how cou-

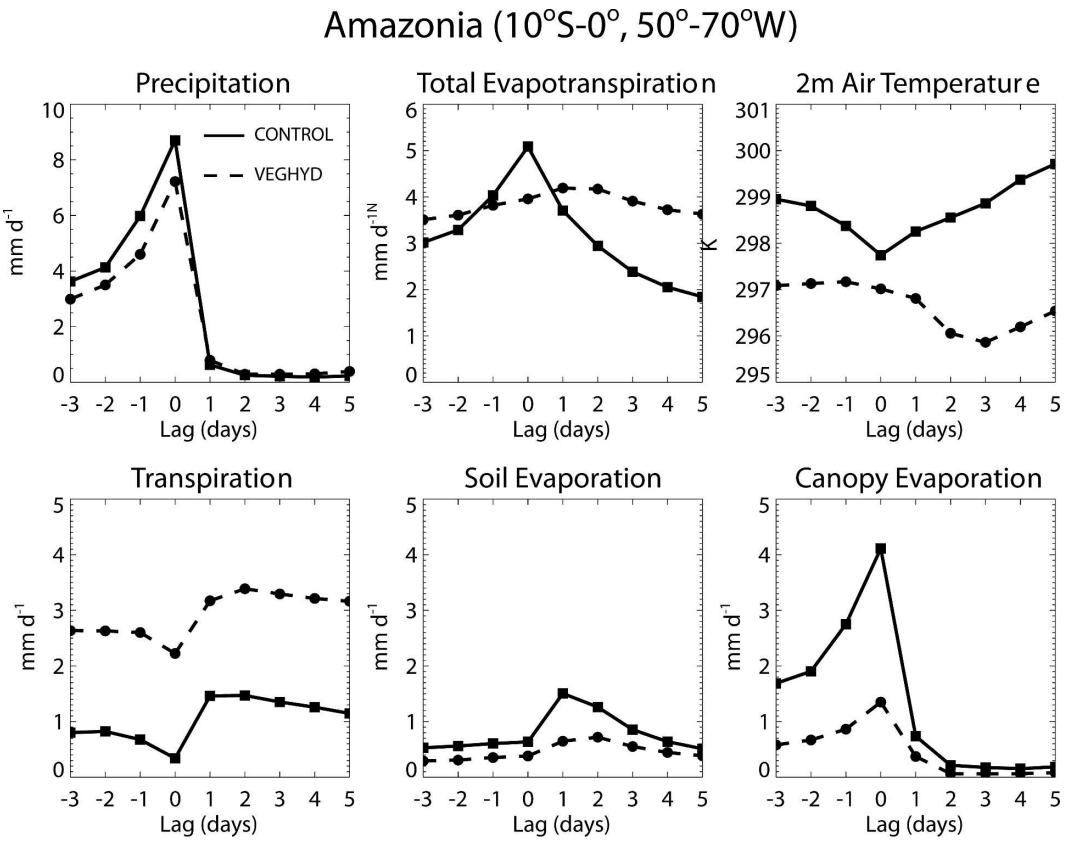

FIG. 11. Same as in Fig. 10, but for Amazonia (10°S–0°, 50°–70°W).

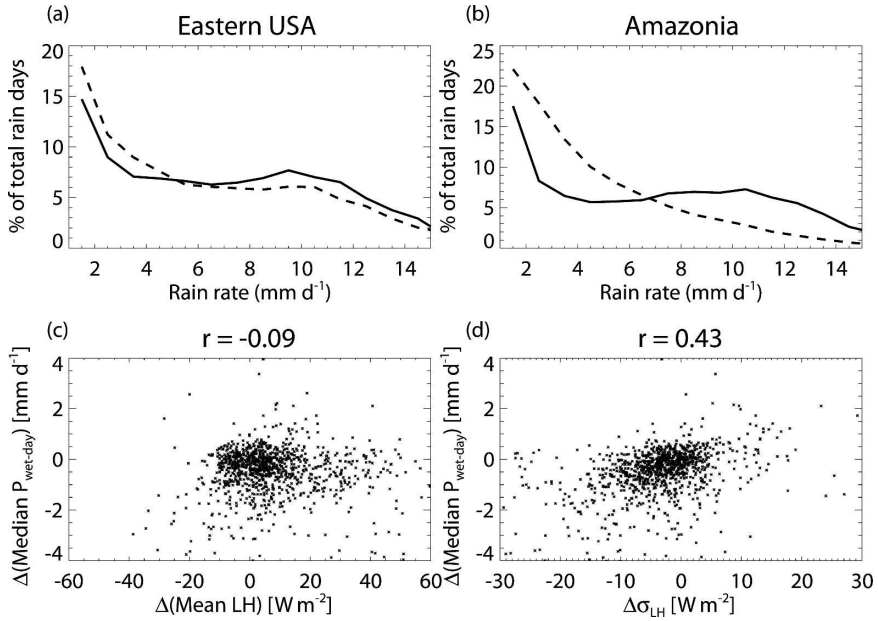

FIG. 12. JJA precipitation distribution, calculated based on daily precipitation from 16 summers, for CONTROL (solid line) and VEGHYD (dashed) for (a) the eastern United States and (b) Amazonia. Scatterplot showing change (VEGHYD − CONTROL) in (c) mean and (d) standard deviation of latent heat flux vs change in median wet-day rain rate. Only nonice, nondesert land grid points are plotted. Correlation coefficients (r) are also shown.

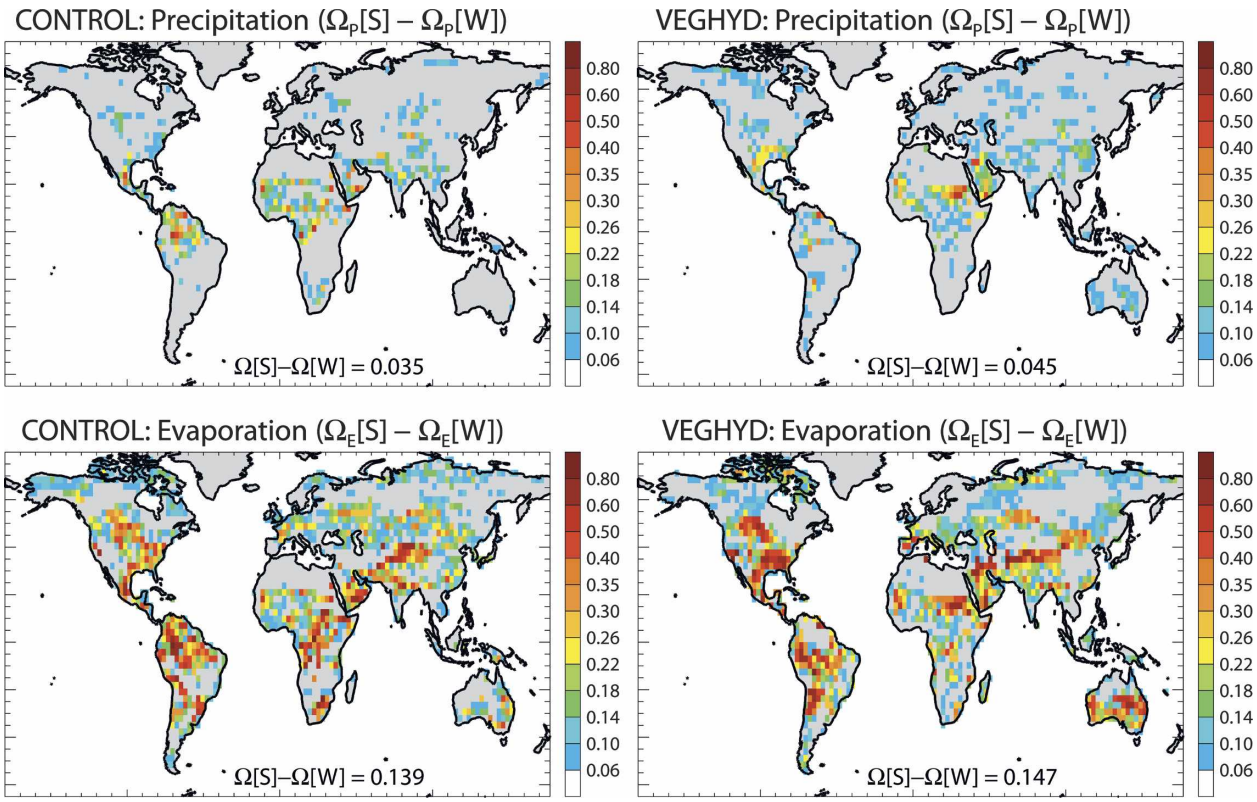

FIG. 13. Global distribution of land–atmosphere coupling strength (Ω[S] − Ω[W]) for (top) precipitation and (bottom) evapotranspiration for CONTROL and VEGHYD experiments. Global average values of $\Delta\Omega$ = Ω[S] − Ω[W] over all nonice land points are shown at bottom of each plot.

pling strength is affected in a version of the model with more reasonable ET partitioning.

Land–atmosphere coupling strength, or the influence of subsurface soil moisture (SM_{sub}) on precipitation (P), is determined in GLACE through an experiment consisting of two ensembles of simulations; the first set is run with a freely evolving land surface (the W ensemble in GLACE) and the second set is forced with subsurface soil moisture taken from one of the W ensemble members (denoted the S ensemble in GLACE). Each ensemble consists of 16 simulations of the same boreal summer (JJA, 1994), with each ensemble member forced with different initial conditions. The similarity of time series across the S or the W ensemble (Ω[S], Ω[W], respectively) varies between 0 (no correlation) and 1 (perfect correlation). We refer the reader to Koster et al. (2006) for more details on the experimental design and calculation of the Ω diagnostic. A land–atmosphere feedback is implied when there is a greater similarity across ensemble member time series in the forced soil moisture ensemble (S) relative to the freely evolving ensemble (W), for example, when $\Delta\Omega$ = Ω[S] − Ω[W] > 0.

The global distribution of land–atmosphere coupling strength for precipitation ($\Delta\Omega_P$) and evapotranspiration ($\Delta\Omega_E$) for CONTROL and VEGHYD is shown in Fig. 13. It is interesting that even though E_T makes up a substantially larger contribution to total ET in VEGHYD, the SM_{sub}–ET relationship is not substantially altered. While there are some regional differences in $\Delta\Omega_E$, particularly in Amazonia, where soil moisture stress on E_T is reduced in VEGHYD leading to a weaker SM_{sub}–ET relationship there, overall the impact of the changes to ET partitioning on the SM_{sub}–ET relationship is modest. Globally averaged values rise only slightly ($\Delta\Omega_E$ = 0.139 in CONTROL; $\Delta\Omega_E$ = 0.147 in VEGHYD). The SM_{sub}–P relationship also strengthens slightly ($\Delta\Omega_P$ = 0.035 in CONTROL; $\Delta\Omega_P$ = 0.045 in VEGHYD).

Global averages of Ω[S] − Ω[W], Ω[S], and Ω[W] over nonice land points for precipitation, ET, 2-m air temperature, E_T, E_S, and E_C are listed in Table 3. The relatively weak impact of the differences in ET partitioning on the SM_{sub}–ET relationship may at least partially be explained by the relatively large influence on Ω[W]; high Ω[W] values are seen when there is a large

TABLE 3. Global average of nonice land points of $\Delta\Omega = \Omega[S] - \Omega[W]$, $\Omega[S]$, $\Omega[W]$ for P, ET, 2-m air temperature (T), E_T, E_S, and E_C.

	$\Delta\Omega = \Omega[S] - \Omega[W]$		$\Omega[S]$		$\Omega[W]$	
Variable	CONTROL	VEGHYD	CONTROL	VEGHYD	CONTROL	VEGHYD
P	0.035	0.045	0.109	0.133	0.075	0.089
ET	0.139	0.147	0.275	0.349	0.136	0.202
T	0.056	0.092	0.356	0.396	0.300	0.303
E_T	0.122	0.132	0.424	0.498	0.302	0.366
E_S	0.141	0.128	0.274	0.329	0.133	0.201
E_C	0.034	0.036	0.196	0.192	0.161	0.157

degree of similarity across the unforced W ensemble time series due to the annual cycle (Koster et al. 2006). For example, $\Omega_{ET}[W]$ is 0.302 in CONTROL and is 0.366 in VEGHYD, reflecting the larger amplitude soil moisture annual cycle and its greater control on E_T. The 0.064 increase in $\Omega_{ET}[W]$ accounts for most of the 0.074 increase in $\Omega_{ET}[S]$ and hence the change in $\Delta\Omega_{ET}$ is only 0.010. This suggests that even though VEGHYD has higher mean E_T, the influence of SM_{sub} anomalies on E_T is roughly equivalent across the two versions of the model. It is interesting that $\Delta\Omega_{ES}$ is roughly the same as $\Delta\Omega_{ET}$ even though soil moisture is specified in the S ensemble only at soil levels deeper than 5 cm. A high $\Delta\Omega_{ES}$ implies that even though the soil moisture in the top soil layers is permitted to evolve freely in the S ensemble, it is modulated by what is happening at deeper levels, presumably through suction of soil water from below when the upper soil is dry and the deep soil is wet and more efficient transfer of water downward when the upper soil is wet and the deep soil is dry.

5. Summary

The partitioning of ET in the control version of CLM3 is poor with global canopy evaporation and soil evaporation far outweighing transpiration, a partitioning that is inconsistent with other offline model estimates. A series of modifications to CLM3 vegetation and soil hydrology parameterizations significantly improve the partitioning of ET, with notable increases seen in transpiration and photosynthesis. The global partitioning is improved in the offline model from 13%, 0.17 mm day^{-1} E_T; 44%, 0.57 mm day^{-1} E_S; and 43%, 0.56 mm day^{-1} E_C to 41%, 0.52 mm day^{-1} E_T; 42%, 0.53 mm day^{-1} E_S; and 17%, 0.21 mm day^{-1} E_C. The broader impact on climate simulations is on the balance beneficial, particularly in the Amazon basin where large biases in dry-season evapotranspiration and air temperatures are sharply reduced. Although the impacts of the new model on mean climate are relatively small, the influence on the nature of the climate simulation is diverse. Stronger transpiration and reduced canopy evaporation result in a more muted and extended ET response to a rain event. In addition, the influence of subsurface soil moisture on precipitation is slightly higher due to increased influence of subsurface soil moisture on transpiration, although the results shown here do not alter the broad conclusions reached in Guo et al. (2006) that convection in CAM3 is overly sensitive to surface heat flux forcing. These analyses confirm the importance of ET partitioning on climate simulations and land–atmosphere interaction in climate models.

Acknowledgments. This study was supported by funding from the U.S. Department of Energy, Office of Biological and Environmental Research, as part of its Climate Change Prediction Program, Cooperative Agreement DE-FC03-97ER62402/A010 and by NASA Earth Science Enterprise, Terrestrial Ecology Program Grant W-19,953 to P. E. Thornton.

REFERENCES

Adler, R. F., and Coauthors, 2003: The Version-2 Global Precipitation Climatology Project (GPCP) Monthly Precipitation Analysis (1979–present). *J. Hydrometeor.,* **4,** 1147–1167.

Allen, S. J., 1990: Measurement and estimation of evaporation from soil under sparse barley crops in northern Syria. *Agric. For. Meteor.,* **49,** 291–309.

Ashktorab, H., W. O. Pruitt, and K. T. Paw U., 1994: Partitioning of evapotranspiration using lysimeter and micro-Bowen ratio system. *J. Irrig. Drain Eng.,* **120,** 450–464.

Baldocchi, D. D., L. K. Xu, and N. Kiang, 2004: How plant functional-type, weather, seasonal drought, and soil physical properties alter water and energy fluxes of an oak-grass savanna and an annual grassland. *Agric. For. Meteor.,* **123,** 13–39.

Beven, K., 1984: Infiltration into a class of vertically non-uniform soils. *Hydro. Sci. J.,* **29,** 425–434.

Black, T. A., and Coauthors, 1996: Annual cycles of water vapour and carbon dioxide fluxes in and above a boreal aspen forest. *Global Change Biol.,* **2,** 219–229.

Bonan, G. B., 1996: A land surface model (LSM version 1.0) for ecological, hydrological, and atmospheric studies: Technical

description and user's guide. NCAR Tech. Note NCAR/TN-417+STR, 150 pp.

——, and S. Levis, 2006: Evaluating aspects of the Community Land and Atmosphere Models (CLM3 and CAM3) using a Dynamic Global Vegetation Model. *J. Climate,* **19,** 2290–2301.

——, K. W. Oleson, M. Vertenstein, S. Levis, X. B. Zeng, Y. J. Dai, R. E. Dickinson, and Z. L. Yang, 2002: The land surface climatology of the community land model coupled to the NCAR community climate model. *J. Climate,* **15,** 3123–3149.

Choudhury, B. J., and N. E. DiGirolamo, 1998: A biophysical process-based estimate of global land surface evaporation using satellite and ancillary data. I. Model description and comparison with observations. *J. Hydrol.,* **205,** 164–185.

——, ——, J. Susskind, W. L. Darnell, S. K. Gupta, and G. Asrar, 1998: A biophysical process-based estimate of global land surface evaporation using satellite and ancillary data. II. Regional and global patterns of seasonal and annual variations. *J. Hydrol.,* **205,** 186–204.

Collins, W. D., and Coauthors, 2006: The formulation and atmospheric simulation of the Community Atmosphere Model version 3 (CAM3). *J. Climate,* **19,** 2144–2161.

Dai, A. G., and K. E. Trenberth, 2002: Estimates of freshwater discharge from continents: Latitudinal and seasonal variations. *J. Hydrometeor.,* **3,** 660–687.

——, ——, and T. Qian, 2004: A global dataset of Palmer Drought Severity Index for 1870–2002: Relationship with soil moisture and effects of surface warming. *J. Hydrometeor.,* **5,** 1117–1130.

Dickinson, R. E., K. W. Oleson, G. Bonan, F. Hoffman, P. Thornton, M. Vertenstein, Z.-L. Yang, and X. Zeng, 2006: The Community Land Model and its climate statistics as a component of the Community Climate System Model. *J. Climate,* **19,** 2302–2324.

Dirmeyer, P. A., X. Gao, M. Zha, Z. Guo, T. Oki, and N. Hanasaki, 2005: The second Global Soil Wetness Project (GSWP-2): Multi-model analysis and implications for our perception of the land surface. COLA Tech. Rep. 185, 46 pp.

Elsenbeer, H., K. Cassel, and J. Castro, 1992: Spatial analysis of soil hydraulic conductivity in a tropical rain forest catchment. *Water Resour. Res.,* **28,** 3201–3214.

Essery, R., M. Best, and P. Cox, 2001: MOSES 2.2 technical documentation. Hadley Centre Tech. Note 30, 30 pp. [Available online at http://www.metoffice.gov.uk/research/hadleycentre/pubs/HCTN/index.html.]

Fekete, B. M., C. J. Vorosmarty, and W. Grabs, 2002: High-resolution fields of global runoff combining observed river discharge and simulated water balances. *Global Biogeochem. Cycles,* **3,** 1042, doi:10.1029/1999GB001254.

Ferretti, D. F., E. Pendall, J. A. Morgan, J. A. Nelson, D. LeCain, and A. R. Mosier, 2003: Partitioning evapotranspiration fluxes from a Colorado grassland using stable isotopes: Seasonal variations and ecosystem implications of elevated atmospheric CO_2. *Plant Soil,* **254,** 291–303.

Gash, J. H. C., C. A. Nobre, J. Roberts, and R. Victoria, 1996: An overview of ABRACOS. *Amazonian Deforestation and Climate,* J. H. C. Gash et al., Eds., John Wiley, 1–14.

Guo, Z., and Coauthors, 2006: GLACE: The Global Land–Atmosphere Coupling Experiment. Part II: Analysis. *J. Hydrometeor.,* **7,** 611–625.

Hack, J. J., J. M. Caron, S. G. Yeager, K. W. Oleson, M. M. Holland, J. E. Truesdale, and P. J. Rasch, 2006: Simulation of the global hydrological cycle in the CCSM Community Atmosphere Model version 3 (CAM3): Mean features. *J. Climate,* **19,** 2199–2221.

Herbst, M., L. Kappen, F. Thamm, and R. Vanselow, 1996: Simultaneous measurements of transpiration, soil evaporation and total evaporation in a maize field in northern Germany. *J. Exp. Bot.,* **47,** 1957–1962.

Hodnett, M. G., M. D. Oyama, J. Tomasella, and A. de O. Marqeus Filho, 1996: Comparisons of long-term soil water storage behavior under pasture and forest in three areas of Amazonia. *Amazonian Climate and Deforestation,* J. H. C. Gash, Ed., John Wiley, 57–78.

Hollinger, S. E., and S. A. Isard, 1994: A soil moisture climatology of Illinois. *J. Climate,* **7,** 822–833.

Koster, R. D., and M. J. Suarez, 2001: Soil moisture memory in climate models. *J. Hydrometeor.,* **2,** 558–570.

——, and Coauthors, 2006: GLACE: The Global Land–Atmosphere Coupling Experiment. Part I: Overview. *J. Hydrometeor.,* **7,** 590–610.

Leuning, R., A. G. Condon, F. X. Dunin, S. Zegelin, and O. T. Denmead, 1994: Rainfall interception and evaporation from soil below a wheat canopy. *Agric. For. Meteor.,* **67,** 221–238.

Liu, Q., and R. E. Dickinson, 2003: Use of a two-mode soil pore size distribution to estimate soil water transport in a land surface model. *Geophys. Res. Lett.,* **30,** 1331, doi:10.1029/2002GL016562.

Malhi, Y., E. Pegoraro, A. D. Nobre, M. G. P. Pereira, J. Grace, A. D. Culf, and R. Clement, 2002: Energy and water dynamics of a central Amazonian rain forest. *J. Geophys. Res.,* **107,** 8061, doi:10.1029/2001JD000623.

Nobre, C. A., G. Fisch, H. R. da Rocha, R. F. F. Lyra, E. P. da Rocha, and B. N. Ubarana, 1996: Observations of the atmospheric boundary layer in Rondônia. *Amazonian Deforestation and Climate,* J. H. C. Gash et al., Eds., John Wiley, 413–424.

Oleson, K. W., and Coauthors, 2004: Technical description of the community land model (CLM). NCAR Tech. Note NCAR/TN-461+STR, 174 pp.

Osborn, T. J., M. Hulme, P. D. Jones, and T. A. Basnett, 2000: Observed trends in the daily intensity of United Kingdom precipitation. *Int. J. Climatol.,* **20,** 347–364.

Qian, T., A. Dai, K. E. Trenberth, and K. W. Oleson, 2006: Simulation of global land surface conditions from 1948 to 2002. Part I: Forcing data and evaluations. *J. Hydrometeor.,* **7,** 953–975.

Robock, A., K. Y. Vinnikov, G. Srinivasan, J. K. Entin, S. E. Hollinger, N. A. Speranskaya, S. X. Liu, and A. Namkhai, 2000: The Global Soil Moisture Data Bank. *Bull. Amer. Meteor. Soc.,* **81,** 1281–1299.

Schlesinger, W. H., 1997: *Biogeochemistry: An Analysis of Global Change*. 2d ed. Academic Press, 588 pp.

Schulze, E. D., F. M. Kelliher, C. Korner, J. Lloyd, and R. Leuning, 1994: Relationships among maximum stomatal conductance, ecosystem surface conductance, carbon assimilation rate, and plant nitrogen nutrition: A global ecology scaling exercise. *Annu. Rev. Ecol. Syst.,* **25,** 629–659.

Shuttleworth, W. J., 1988: Evaporation from Amazonian rainforest. *Proc. Roy. Soc. London,* **233,** 321–346.

Thornton, P. E., and N. Zimmerman, 2007: An improved canopy integration scheme for a land surface model with prognostic canopy structure. *J. Climate,* **20,** 3902–3923.

Vinnikov, K. Ya., and I. B. Yeserkepova, 1991: Soil moisture: Empirical data and model results. *J. Climate,* **4,** 66–79.

Wallace, J. S., C. R. Lloyd, and M. V. K. Sivakumar, 1993: Measurements of soil, plant and total evaporation from millet in Niger. *Agric. For. Meteor.,* **63,** 149–169.

Werth, D., and R. Avissar, 2004: The regional evapotranspiration of the Amazon. *J. Hydrometeor.,* **5,** 100–109.

Williams, D. G., and Coauthors, 2004: Evapotranspiration components determined by stable isotope, sap flow and eddy covariance techniques. *Agric. For. Meteor.,* **125,** 241–258.

Willmott, C. J., and K. Matsuura, cited 2000: Terrestrial air temperature and precipitation: Monthly and annual climatologies. [Available online at http://climate.geog.udel.edu/~climate.]

Wilson, K. B., P. J. Hanson, P. J. Mulholland, D. D. Baldocchi, and S. D. Wullschleger, 2001: A comparison of methods for determining forest evapotranspiration and its components: Sap-flow, soil water budget, eddy covariance and catchment water balance. *Agric. For. Meteor.,* **106,** 153–168.

Wu, W. R., and R. E. Dickinson, 2004: Time scales of layered soil moisture memory in the context of land–atmosphere interaction. *J. Climate,* **17,** 2752–2764.

Yunusa, I. A. M., R. R. Walker, and J. R. Guy, 1997: Partitioning of seasonal evapotranspiration from a commercial furrow irrigated Sultana vineyard. *Irrig. Sci.,* **18,** 45–54.

Zeng, X., R. E. Dickinson, M. Barlage, Y. Dai, G. Wang, and K. Oleson, 2005: Treatment of undercanopy turbulence in land models. *J. Climate,* **18,** 5086–5094.